Cerebral Cortex, October 2018;28: 3429–3444

doi: 10.1093/cercor/bhx206
Advance Access Publication Date: 11 August 2017
Original Article

ORIGINAL ARTICLE

Cortical Auditory-Evoked Responses in Preterm Neonates: Revisited by Spectral and Temporal Analyses

A. Kaminska[1,2], V. Delattre[1,3], J. Laschet[1], J. Dubois[4], M. Labidurie[1], A. Duval[1,3], A. Manresa[5], J.-F. Magny[6], S. Hovhannisyan[6], M. Mokhtari[7], L. Ouss[8], A. Boissel[5], L. Hertz-Pannier[1,3], M. Sintsov[9], M. Minlebaev[9,10], R. Khazipov[9,10] and C. Chiron[1]

[1]INSERM U1129, 75015 Paris, France; Paris Descartes University, Sorbonne Paris Cité, 75005 Paris, France; CEA, 91191 Gif sur Yvette, France, [2]Department of Clinical Neurophysiology, AP-HP, Necker-Enfants Malades Hospital, 75015 Paris, France, [3]Neurospin, UNIACT, CEA, 91191 Gif sur Yvette, France, [4]INSERM U992, CEA/DRF/I2BM/Neurospin/UNICOG, 91191 Gif-sur-Yvette, France; Paris Saclay University, Paris-Sud University, 91191 Gif-sur-Yvette, France, [5]Laboratory of Psychology and Neurosciences (LPN) (EA 47000), Rouen University, Rouen 76000, France, [6]Neonatal Intensive Care Unit, AP-HP, Necker-Enfants Malades Hospital, 75015 Paris, France, [7]Neonatal Intensive Care Unit, AP-HP, Bicetre Hospital, 94270 Kremlin-Bicetre, France, [8]Department of Pediatric Neurology, AP-HP, Necker-Enfants Malades Hospital, 75015 Paris, France, [9]Laboratory of Neurobiology, Kazan Federal University, 420012 Kazan, Russia and [10]INSERM U901/ INMED, Aix-Marseille University, 13009 Marseille, France

Address correspondence to Anna Kaminska, Department of Clinical Neurophysiology, Necker-Enfants Malades Hospital, 149 rue de Sèvres, 75015 Paris, France. Email: anna.kaminska@aphp.fr

Abstract

Characteristic preterm EEG patterns of "Delta-brushes" (DBs) have been reported in the temporal cortex following auditory stimuli, but their spatio-temporal dynamics remains elusive. Using 32-electrode EEG recordings and co-registration of electrodes' position to 3D-MRI of age-matched neonates, we explored the cortical auditory-evoked responses (AERs) after 'click' stimuli in 30 healthy neonates aged 30–38 post-menstrual weeks (PMW). (1) We visually identified auditory-evoked DBs within AERs in all the babies between 30 and 33 PMW and a decreasing response rate afterwards. (2) The AERs showed an increase in EEG power from delta to gamma frequency bands over the middle and posterior temporal regions with higher values in quiet sleep and on the right. (3) Time–frequency and averaging analyses showed that the delta component of DBs, which negatively peaked around 550 and 750 ms over the middle and posterior temporal regions, respectively, was superimposed with fast (alpha–gamma) oscillations and corresponded to the late part of the cortical auditory-evoked potential (CAEP), a feature missed when using classical CAEP processing. As evoked DBs rate and AERs delta to alpha frequency power decreased until full term, auditory-evoked DBs are thus associated with the prenatal development of auditory processing and may suggest an early emerging hemispheric specialization.

Key words: auditory-evoked potentials, Delta-brushes, early gamma oscillations, high-density EEG, preterm.

Introduction

Whereas fetal brain activity is hardly accessible, EEG recording in the preterm-born human neonate discloses developmental and transitory patterns thought to reflect the progressive organization of fetal brain networks. Indeed, sequential changes have been shown closely linked to gestational age during the equivalent last 3 months of pregnancy (Curzi-Dascalova et al. 1993; Vanhatalo et al. 2005; André et al. 2010; Koolen et al. 2015, 2016). The precise description of such immature activity patterns has tremendous implications for both the understanding of underlying connectivity and the development of neurophysiological markers of normal and potentially abnormal networks in this highly vulnerable period of life. Although these patterns have been extensively studied in rodents (for review see Luhmann et al. 2016), they remain incompletely known in humans.

The most frequent preterm EEG patterns in humans have been originally designed as "Delta-brushes" (DBs) (Lamblin et al. 1999), then reported as Slow endogenous Activity Transients (SATs) (Vanhatalo et al. 2005). SATs were described using full bandwidth EEG (0–50 Hz) and consist of large slow voltage deflections (0.1–0.5 Hz, up to 800 μV) with bursts of fast oscillations (up to 30 Hz) (Vanhatalo et al. 2005; Koolen et al. 2016). DBs actually correspond to the same grapho-elements, however, distorted after the cut-off of infra-slow wave component by conventional 0.53 Hz high-pass filtering (Lamblin et al. 1999; Vanhatalo and Kaila 2006). DBs consist of high amplitude delta band slow waves (50–300 μV) superimposed with rapid oscillations (>8 Hz) (André et al. 2010). In sensory cortices, DBs appear to be partly elicited by various sensory stimulations, for instance in central cortical regions by spontaneous hand or foot twitches, or even tactile stimulation, in a somatotopic manner (Milh et al. 2007; Fabrizi et al. 2011; Stjerna et al. 2012). We showed that before 35 post-menstrual weeks (PMW), light flashes and auditory stimuli (words and "clicks") evoke DBs in occipital and temporal regions respectively (Colonnese et al. 2010; Chipaux et al. 2013).

Prior studies in rats had demonstrated that during the first neonatal weeks (comparable to the third trimester of human gestation), the thalamo-cortical loop responds to a sensory input with a burst of rapid oscillations nested in a slow wave, a complex grapho-element called "spindle-burst" (SBs). Homology between SBs and DBs has been suggested, supported by the same sensitivity to sensory input, a comparable frequency characteristics and a similar developmental profile, both disappearing at the end of the second postnatal week and at term, respectively (Milh et al. 2007; Khazipov et al. 2013; Luhmann et al. 2016; Yang et al. 2016). SBs are driven by sensory feedback resulting from myoclonic twitches and whisker stimulation in somatosensory cortex, and from retinal waves in visual cortex (Khazipov et al. 2004; Hanganu et al. 2006; Khazipov and Luhmann 2006; Minlebaev et al. 2007, 2011; Yang et al. 2009, 2013; Hanganu-Opatz 2010; Tiriac et al. 2012). A growing body of experimental studies has provided in depth information about SBs mechanisms: in particular, they contain early gamma oscillations (EGOs) that (1) are primarily driven by rhythmic gamma excitation from the thalamus, (2) enable millisecond-precise temporal binding of the topographically aligned thalamic and cortical neurons, and (3) support long-term dependent potentiation in the thalamo-cortical synapses (Minlebaev et al. 2007, 2011; An et al. 2012, 2014; Khazipov et al. 2013; Yang et al. 2013).

However, the spatio-temporal dynamics of preterm sensory-evoked DBs still remain elusive in humans. In the fetus and preterm baby, the first cortical sensory-evoked responses (somatosensory, visual, auditory) have been described from 24PMW on, when the first thalamo-cortical afferents reach the cortical plate after a waiting period in the subplate (Kostovic and Judas 2006; Wunderlich and Cone-Wesson 2006). In the auditory system, responses were mainly studied using the methodology of "evoked potentials" that averages up to a hundred responses evoked by clicks 70 dB above the hearing level, thus smoothing the high frequency components not time-locked to the stimulus (Weitzman et al. 1967; Desmedt and Manil 1970; Hrbek et al. 1973; Rotteveel et al. 1987a, 1987b; Picton et al. 1999). Therefore, our objectives were (1) to characterize in detail the frequency spectrum and spatio-temporal dynamics of preterm AERs, and (2) to compare them with previously reported cortical auditory-evoked potentials (CAEPs) in preterm infants (Weitzman et al. 1967; Rotteveel et al. 1987a, 1987b).This could hardly be achieved in our previous study that used standard recording setup (9 electrodes) and low intensity clicks (20 dB) (Chipaux et al. 2013). In the present study of 30–38 PMW neonates, we improved the spatio-temporal resolution of AERs using higher density EEG (32 electrodes) and registration of electrode positions to 3D reconstructions of preterm head and brain computed from MRI of age-matched groups.

Materials and Methods

Participants

All premature infants referred to the neonatal intensive care units (NICU) of Necker-Enfants Malades (Paris, France) and Bicêtre Hospital (Kremlin–Bicêtre) from October 2013 to April 2014 and from November 2014 to December 2014 were prospectively screened for inclusion. To include only neonates without neurological risk, inclusion criteria were as follows: age over 7 days, normal delivery, birth weight over the 10th percentile, spontaneous ventilation (nasal positive pressure was accepted), normal clinical examination, normal ultrasound scan performed by a pediatric radiologist (intraventricular hemorrhage grade I-II was accepted), normal otoacoustic emissions, no postnatal steroid treatment and no sedative drug within less than 4 days before the recording. EEGs were performed as part of routine neurological follow-up according to the recommendations for premature infants (André et al. 2010), at patients' bedside. Infants were prospectively followed by a trained neonatologist at 6 months, 1 year, and 2 years, and were secondarily excluded from the analysis if psychomotor and neurological development was abnormal (1 case). Written informed consent was obtained from all parents. The procedure was in accordance with the Ethics Code of the World Medical Association, was approved by our institutional review board, INSERM (French National Institute of Medical Research) Ethics Committee, and was registered as a Clinical Research Study classified within "methodology of reference" under the n° 558/BB/PA/2005-12 (available on The French National Research Agency site as ANR-09-MNPS-006-01 « DB »).

Thirty neonates were investigated including 7 pairs of twins. Gestational age at birth (weeks of gestation) was 26–27 (n = 3), 29–30 (n = 2), 31–32 (n = 11), 33–34 (n = 13), and 35–36 (n = 2). Age at recording was expressed as postmenstrual weeks (PMW = gestational age at birth + postnatal weeks). Clinical follow-up (showing normal development) was performed at 2 years for 18 infants, at one year for 5 infants; 7 infants were lost to follow-up.

EEG Recording and Auditory Stimuli

Recordings were performed at the following PMW: 30–31 (n = 2), 32–33 (n = 8), 34–35 (n = 8), and 36–38 (n = 12), according to the

10/10 international system and using 32 electrodes neonatal caps (Wave Guard EEG neonatal cap, ANT-Neuro, certification CE, 3 sizes, Fig. 1A). They included cardiogram and respiration recording. Signals were sampled at 1024 Hz, amplified (1000×), band-pass filtered at 0.16–334 Hz and digitized, using the Deltamed Coherence EEG system. Offline analysis was performed using the Coherence review program (Deltamed/Natus Paris) and Matlab (Mathworks).

Auditory stimuli were generated with the Centor Auditory-Evoked potential device (Deltamed France) and presented with constant sound volume via headphones (Fig. 1A). The direct current (DC) output from the Centor was connected to a DC input of the amplifier, allowing insertion in the EEG recording of markers at the onset of the stimulus. The stimulus consisted of a conventional 100μs rectangular unfiltered alternating Click (Centor device for CAEP) at 70 dB hearing level, presented binaurally every 10 s (Robles and Ruggero 2001; Guideline 9C, 2008). Since auditory-evoked responses (AERs) require to be recorded when the infant is perfectly quiet to avoid movement artifacts, stimuli were initiated as soon as the infant fell asleep, and they were repeated until he woke up. EEG recording lasted no more than 1 h. The number of recorded auditory stimuli therefore depended on sleep duration. Moreover, as EEG must be free of any artifacts during the response period, the mean number of

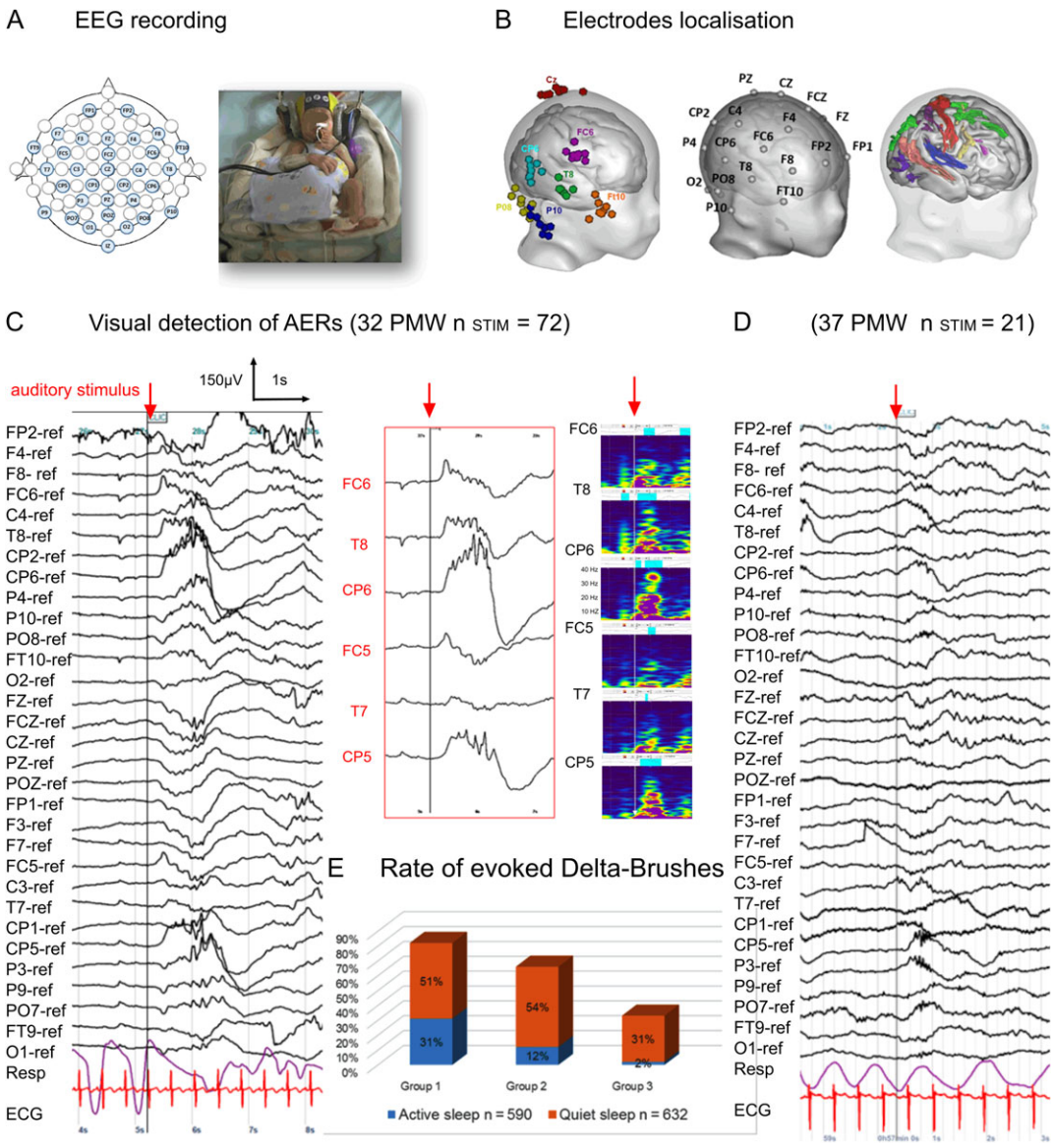

Figure 1. EEG recording, localization of the electrodes position and visual detection of AERs. (*A*) Shematic representation of the 32 electrodes of the Wave Guard EEG neonatal cap, according to the 10/10 international system (left) and recording installation in a 32 PMW neonate (right). (*B*) Registration of the electrodes of interest for the 8 neonates aged 32–33 PMW to the head scalp and brain of an age-matched subject (left); average positions of electrodes in the group 30–33 PMW ($n = 8$) (middle, for detail see Supplementary Table 2); cortical sulci of the 5 neonates of the 32–33 PMW MRI group superimposed to the head scalp and the inner cortical surface of an age-matched new-born group (right, for detail see Supplementary Fig.1). (*C*) EEG with mean reference montage(high-pass filter: 0.53 Hz, notch filter: 50 Hz) in a 32 PMW neonate showing representative examples of DBs evoked by an auditory "click" during QS; upward deflection represents negative potential (left) and zoom on the electrodes of interest (FC6, T8, CP6, outlined in red) of the auditory-evoked DBs shown on the left (middle); corresponding wavelet analyses at outlined electrodes (right). (*D*) EEG with mean reference montage (high-pass filter: 0.53 Hz, notch filter: 50 Hz) in a 37 PMW neonate. (*E*) Rate of evoked DBs assessed by visual analysis in active and QS according to age groups.

analyzable stimuli was of 41 ± 35 (see Supplementary Table 1) after screening of all responses.

EEG Signal Analysis

Localizing the Electrodes' Position

MRI examination could not be obtained in these healthy neonates, preventing us from registering the electrodes position on the infant's own MRI, as considered optimal (Kabdebon et al. 2014). As digitalization of anatomical landmarks and electrodes was impossible at the infant's bedside, we opted for an alternative strategy based on individual foam head moldings with annotated scalp landmarks, enabling the secondary digitalization of electrodes positions as well as of a hundred random head scalp points. Besides, to localize the electrodes' position with respect to brain anatomy, we created 3D MR reconstructions of scalps and cortical surfaces (with primary sulci) from other neurologically healthy infants, considering 3 age groups: 32–33 PMW, 34–35 PMW, and 38–40 PMW. Each individual head model was further registered to the age-matched MRI template using head scalp landmarks (see details in Supplementary Material 1, Supplementary Fig.1, and Supplementary Table 2).

Visual Detection of AERs (Auditory-Evoked DBs)

EEG recording was first visually analyzed by a trained pediatric neurophysiologist (A.K.), to confirm normality. Artifact-free time intervals were selected manually for further analyses. All stimuli annotations were checked and stimuli with EEG artifacts within 2 s before and 2 s after the stimulus were excluded from the analysis. Quiet sleep (QS) was assessed by discontinuous, semi-discontinuous or "tracé alternant" EEG according to PMW, regular respiration and cardiac rhythms, with absence of phasic movements disclosed by EEG artifacts and/or concomitant video recording. Active sleep (AS) was characterized by continuous activity, irregular respiration, and phasic movements (André et al. 2010). Each stimulus was assigned a concomitant sleep stage. Auditory-evoked DBs were searched for visually on raw EEG (by AK) for each selected artifact-free stimulus. The rate of evoked DBs (number of evoked DBs within 2 s after the stimulus/ number of stimuli) was determined in each infant according to sleep stage (Supplementary Table 1). Evoked DBs were considered as "easily identifiable" if the rate was >30%.

Frequency Power Spectrum Analysis of AERs

The frequency power spectrum immediately preceding and following auditory stimuli was compared, for each electrode, over a 2 s time interval using the Fast Fourier Transform algorithm with 0.5 Hz frequency resolution and mean reference (Coherence, FFT analysis, Natus). Power spectra were broken into 6 frequency bands (delta: 0.5–3.5 Hz, theta: 4–7.5 Hz, alpha: 8–13 Hz, beta: 13.5–31.5 Hz, gamma 1: 31.5–48 Hz; gamma 2: 52–80 Hz). Notch filter of 4 Hz was used at 50 and 100 Hz to avoid artifacts from sector and its harmonics. Data were analyzed using the acquisition software (Coherence, FFT analysis). Considering the huge number of comparisons, several alpha-errors (0.05, 0.01, 0.001, and 0.0001) were simultaneously examined in a single view (color-coded maps) to balance gain in random effects and loss in specific effects.

For individual analysis, positive effects were considered as stimuli-specific when the highest power increase ratio after the stimulus was recorded on at least one temporal electrode (CP5-CP6 or T7-T8) and in at least 3 frequency bands as previously described (Chipaux et al. 2013). Positive effects had a great risk to be random when they were both topically isolated (recorded by a single electrode other than those defined above) and visible in a single frequency band. In this analysis, the classical Bonferroni adjustment was not applicable as it clearly erased stimulus-specific effects in almost all patients. For most patients, however, we found by stepwise lowering the alpha error from 0.05 to 0.0001 that the random effects defined above vanished when alpha was set to 0.01 (or lower). This arbitrary chosen setting is equivalent to a 5-fold Bonferroni adjustment, and did not affect the stimulus-specific responses. Population/group statistical analysis was performed calculating ratios after data averaging (over all stimuli for each new-born) and Log-transformation, and using multiple linear regression model (least squares fitting) by including all electrodes and the age (PMW) as variables of interest. Data were further analyzed for interaction, using a model including the cross effects between electrodes as a factor and other variables of interest (sleep stage, age in PMW, and number of stimulations). To search for lateralization left and right homologous electrodes were compared for their relative effects (where at least one was found significant) using paired *t*-test.

Maturational changes in AERs were further assessed by analyses within 30–38 PMW age groups. Based on previous studies in preterm infants showing a power decrease at 34–35 PMW related to a decrease in DBs occurrence, along with a modification of CAEP morphology (Weitzman et al. 1967; Rotteveel et al. 1987a, 1987b; Wunderlich and Cone-Wesson 2006; Chipaux et al. 2013), we split the population into 3 groups: 30–33 PMW (group 1, $n = 10$), 34–35 PMW (group 2, $n = 8$), and 36–38 PMW (group 3, $n = 12$). Two possible confounding factors related to the number of stimulations and sleep stage could interact globally with age. Newborns fall asleep in the AS and hence the interval from the beginning of recording to the first QS period is variable (ranging from 0 min to 1 h), thus the number of stimuli per infant and per sleep stage was highly variable (Curzi-Dascalova et al. 1993). We therefore selected the first 21 stimulations (21 being the mean number of stimulations in group 2, which had the lowest number of stimuli) beginning when the child fell asleep, so that the number of stimuli was comparable between age groups and stimulations fell mostly in the AS for all babies. For each of the 3 age groups, the same population analyses were performed. Additionally, a paired *t*-test was performed for each electrode and for each frequency band on the means of the Log-transformed values before and after stimulation obtained over n stimulations. The default alpha error was set to 0.05 for the population/group analyses. All statistical procedures were performed using the JMP v.12 software (SAS Institute Inc.).

Continuous Time–Frequency Wavelet Analysis of AERs

Based on the absence of EEG artifacts and presence of gamma activity on spectral analysis, EEG recordings of 7 babies of different ages (aging PMW30–37) were used. As previously described, raw data were pre-processed involving notch filtering (centers at 50, 100, 150, 200, 250 Hz), band-pass window of 4 Hz, and whole-scalp electrode re-referencing. Recordings were checked by 2 operators (A.K., M.M.) and stimuli with uncorrected artifacts were rejected manually. Detection of AER was done in 2 steps. Firstly, the significance of the AER (EEG deflection following the stimulus) was calculated independently for each electrode. AER deflection was considered significant if the amplitude distribution of the averaged EEG signal at a given electrode significantly differed between the 1 s periods

before and after the auditory stimulus (Student's *t*-test, $P < 0.05$). Next, the amplitude of the AER was calculated on the electrodes showing a significant response by measuring the difference in peak amplitudes between the AER and the 1 s pre-stimulus EEG period. Then, continuous wavelet transform was applied on the 6 s EEG segments centered on the stimulus. However, to exclude edge artifacts, only 4 s (±2 s around auditory stimulus) was used for further analysis. Given the oscillatory nature of the AER, Morlet wavelet was chosen with several center frequencies (80 Hz, 40 Hz, 20 Hz, 10 Hz, 5 Hz, 2.5 Hz, 1.25 Hz, and 0.625 Hz) to cover the frequency bands of interest and to maintain wavelets independency. For each frequency range, we considered that activity was present when all post-stimulus wavelet coefficients exceeded 3 standard deviations of the mean pre-stimulus coefficients. The segments with significant oscillatory episodes underwent a morphological opening and closing for each wavelet coefficient (the kernel size was matched to the wavelet characteristics that resulted in reconstruction of the continuous episode of oscillatory activity). Reconstruction of the gamma oscillation with central frequency of 80 Hz failed to produce the significant evoked response, thus the oscillatory response in this frequency range was excluded from further analysis.

Based on center frequency, the detected oscillatory events were labeled as "Delta" (0.625 Hz or 1.25 Hz or 2.5 Hz), "Theta" (5 Hz), "Alpha" (10 Hz), "Beta" (20 Hz), and "Gamma" (40 Hz) oscillations. Two patterns were also distinguished: "Brush" (the presence of "Alpha" and "Beta" components) and "DB" (the presence of "Delta" and "Brush" components). The probability of appearance, spatial and time distributions were calculated using time stamps of the significant wavelet coefficients of the model oscillations in different frequency bands. To compute temporal characteristics (onset, offset, and duration) of the evoked oscillatory components in different frequency ranges, the time distributions for each oscillation type were characterized: onset and offset were identified as the distribution excesses of 25 and 75%, respectively, and the oscillation duration was the interval in-between. The analysis was done using EEGLAB toolbox (Delorme and Makeig 2004) and Wavelet toolbox in MATLAB. Group measures were expressed as means ± standard deviation. Paired Student's *t*-test for each experiment was used to assess the statistical significance of differences (1) between different electrodes in the analysis of the spatial distribution of AERs and (2) of frequency components of the AERs based on the analysis of the pre- and post-stimuli EEG traces. The level of significance was set at $P < 0.05$.

Cortical Auditory-Evoked Potentials

To understand the relationships between the auditory-evoked DBs and the classical CAEPs within AERs, we analyzed the topographic and morphologic characteristics of the slow components of AERs with reference to previous studies of CAEPs in premature infants (Weitzman et al. 1967; Rotteveel et al. 1987a, 1987b). Stimulus "click" locked averaging of individual recordings was performed for each electrode using the Coherence review program (Deltamed/Natus Paris, France). The analysis window was of 5 s with a baseline of 2 s. Latency was measured from the stimulus onset to the wave peak and amplitude from the baseline to the wave peak. To minimize signal distortion and as recommended for waveform analysis of event-related potentials, for power spectrum analysis and for high-density recordings we used the minimal high-pass filter (0.16 Hz) of our EEG device and a mean reference since non-neutral reference to the mastoid or vertex might induce a systematic bias (Qin et al. 2010; Acunzo et al. 2012; Tanner et al. 2015).To further identify CAEPs peaks and compare to previously described CAEPs in premature infants we measured the peaks of the waves at midline (FZ, CZ), lateral frontal-central (FC5, FC6), and temporal (T7, T8, CP5, CP6) electrodes using a 1.59 Hz high-pass filter and reference at the level of P9 and P10 electrodes (located near the mastoid) (Weitzman et al. 1967; Rotteveel et al. 1987a, 1987b; Wunderlich and Cone-Wesson 2006). Since our EEG device did not allow to apply 1 Hz (used in the normative data for CAEP), we used 1.59 Hz high-pass filter for this comparison. Latencies and amplitudes were expressed with mean and standard deviation and compared (regarding age groups, high-pass filter, reference site and topography) using 2-tailed *t*-test. CAEPs were represented at all electrodes of the EEG trace of averaged AERs and using 2D and 3D EEG mapping. 3D EEG mapping was built using the mean position of digitalized electrodes co-registered to the head scalp of a single age-matched subject. The value of EEG potential (μVolts) was represented at each electrode at a given time (represented by time cursor) and according to reference and filters used. In each vertex of the scalp model (notably between electrodes), the EEG potential was interpolated as the weighted sum of the neighbor electrode potentials. Since CAEP revealed a sequence of successive slow waves at neighboring electrodes, we aimed to estimate the propagation speed of these waves, dividing the mean distances between electrodes by the mean time lag between the respective peaks (in milliseconds). Age-related changes were examined by considering the same 3 age groups as previously.

Results

Localizing the Electrodes Position

Our 32-electrode caps provided a good spatial coverage, especially for the youngest infants with a 25–30 mm distance between the central points of neighbouring electrodes (for comparison the diameter of skin contact area was 5 mm). The electrodes of interest for AERs disclosed negligible topographic variability within each age group so that their localization could be satisfactorily assessed (Fig. 1B; Supplementary Fig. 1, see details in Supplementary Material 1 and Supplementary Table 2). In particular, temporal electrodes (T7-8 and CP5-6, respectively) overlaid the middle temporal and posterior temporal regions near the temporo-occipital junction, while CP1–2 electrodes overlaid the parieto-temporo-occipital junction, C3-4 electrodes the post-central inferior region, and FC5-6 electrodes the inferior pre-central region (Supplementary Table 2, Fig. 1B, Supplementary Fig. 1).

Visual Detection of AERs (Auditory-Evoked DBs)

Auditory-evoked DBs were detected in 25 babies (83% of the whole population) (see Supplementary Table 1). Nine of them had a response rate ≤30%, leaving 16 babies with easily visually identifiable DBs (53% of the whole population). In Group 1 (30–33 PMW) all babies had easily identifiable DBs, mostly in QS (Fig. 1C; Supplementary Table 1). DBs consisted of a high amplitude slow wave with superimposed rapid rhythms, located on FC5-6, T7-8, CP6-7 electrodes, and often beginning with a negative peak in the theta band mostly on FC5-6 or T7-8 electrodes (Fig. 1C). From around 35 PMW on, evoked temporal DBs were less apparent and smaller in amplitude or evoked responses were more diffuse without clear temporal focalization (Fig. 1D). Their mean response rate during QS and AS decreased with age

from 51 to 31% at 31–33 PMW to 31 and 2% at 36–38 PMW, respectively (Fig. 1E).

Frequency Power Spectrum Analysis of AERs

a. Population analysis showed a significant increase of frequency power in most frequency bands on CP5-6 and T7-8 electrodes (see Supplementary Fig. 2A details statistical results). The power increase was significantly higher in QS than in AS in delta to gamma 1 bands ($P < 0.0001$). The highest power increase was observed on CP6 and T8 in all 5 frequency bands. Significant power increase was also observed on CP5 electrode in delta, alpha, and beta bands, and on T7 in delta to beta bands. Other electrodes also showed significant power increase, such as CZ (theta to beta bands) and FP1 (delta and theta bands) (see Supplementary Fig. 2A). When left and right homologous electrodes showing a significant increase of frequency power were compared (CP5-CP6, T7-T8), we observed a right predominance ($P < 0.0001$).
b. Individual analysis showed a significant increase of frequency power on temporal electrodes in 17 infants (56% of the whole population, 80% of the youngest group (see Supplementary Table 1, Supplementary Fig. 2B). Among them, all but one also had visually identifiable DBs.
c. Power increase after auditory stimulus in each age group also predominated on the right temporal electrodes (Fig. 2), however, we found a more diffuse response, including significant power increase in the delta band on vertex electrodes and in delta to beta on P9 and P10 (near the mastoid electrode) in groups 1 and 3 (Fig. 2). Increasing the number of stimulations significantly increased the power on CP5 and CP6 electrodes ($P < 0.05$), whereas post-stimulation power increase significantly decreased with age in delta to alpha bands ($P < 0.01$).

Continuous Time–Frequency Wavelet Analysis of AERs

EEG recordings of 7 preterm infants aged 30–37 PMW were selected from the whole population according to 3 criteria: (1) evoked activity in the gamma frequency band (2) representation of candidates from all age groups and (3) the absence of strong artifacts affecting continuous time–frequency analysis. Analysis of evoked AERs showed the presence of negative and positive deflections associated with auditory stimulation (Fig. 3A). The spatial distribution of AERs was nonuniform but rather concentrated in bilateral regions, on CP5 and CP6 electrodes ($55 \pm 21\,\mu V$ and $62 \pm 13\,\mu V$, respectively; Fig. 3B–E; $n = 7$; $P < 0.05$). Higher amplitude of the AERs was associated with a larger number of EEG channels recording significant AERs above the right hemisphere ($n = 7$; Fig. 3F). The number of significant detections revealed side differences: on the left

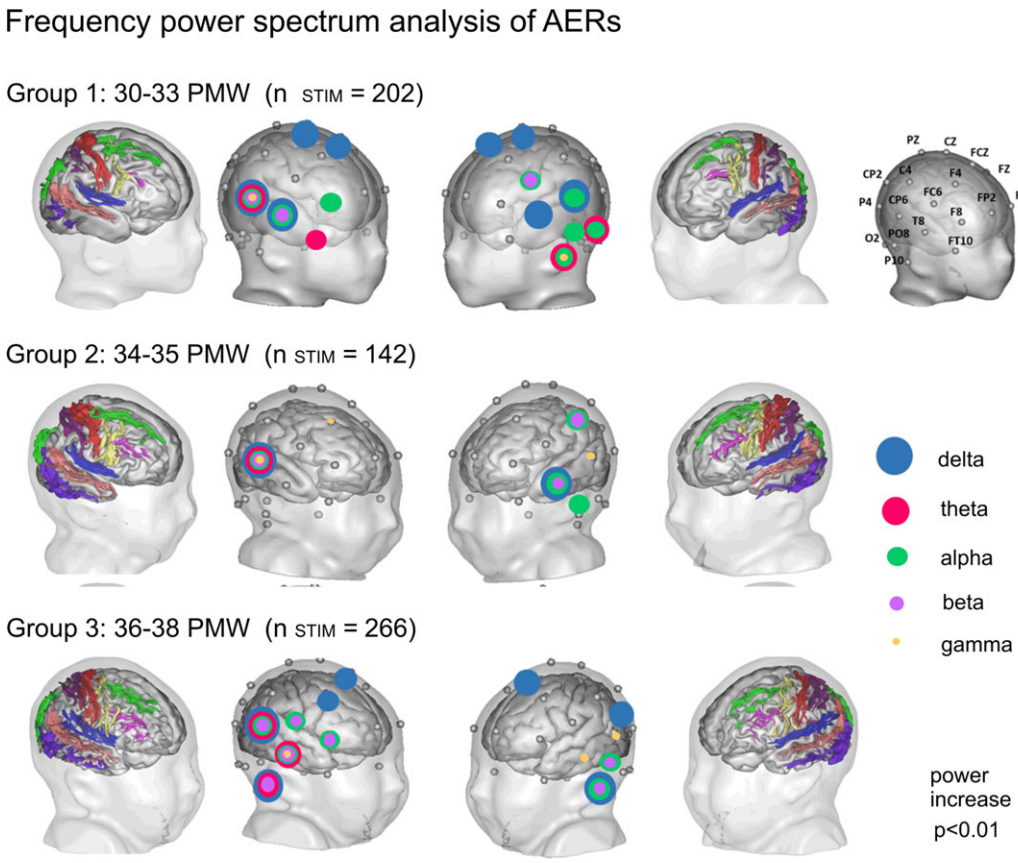

Figure 2. Frequency power spectrum analysis of AERs in regards to the mean position of digitalized electrodes co-registered to the head scalp and brain of age-matched subjects. Power increase is shown in each age group, for each electrode and in the 5 frequency bands (delta: 0.5–3.5 Hz, theta: 4–7.5 Hz, alpha: 8–13 Hz, beta: 13.5–31.5 Hz, gamma 1: 31.5–48 Hz). Colour circles show the electrodes with a significant increase of power ratio at $P < 0.01$. The main primary sulci are represented on each hemisphere: the posterior lateral fissure (blue), the central sulcus (red), the superior temporal sulcus (light pink), the inferior temporal sulcus (purple), the inferior frontal sulcus (fuchsia), the superior frontal sulcus (green), the pre-central sulcus (yellow), the post-central sulcus (heather purple), and the intraparietal sulcus (green).

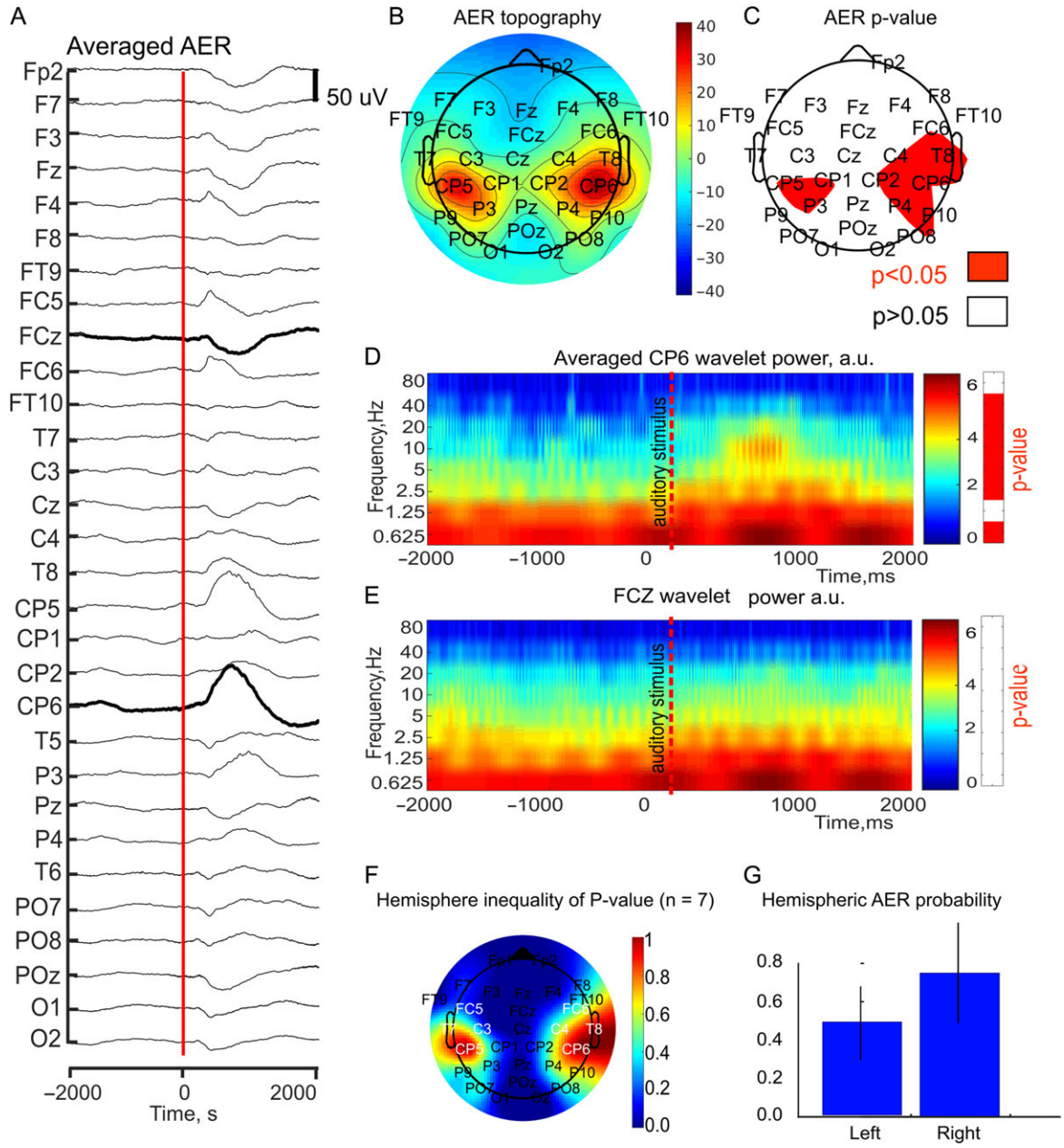

Figure 3. AER analysis in time and time–frequency domain. (*A*) 32 electrodes sweep-averaged EEG activity triggered by auditory stimulus (red line). (*B*) Spatial representation of the AER calculated as the time-averaged 2 s post-stimulus EEG value referenced to the time-averaged 2 s pre-stimulus value. (*C*) *P*-value map of the spatial distribution of the AER shown on *B*. (*D* and *E*) Averaged wavelet scalogram for the example shown in *A* for the electrodes with significant (*D*) and nonsignificant (*E*) AER. Color coding represents logarithmic power of recorded EEG examples. The bars on the right indicate the significant EEG difference of the post-stimulus when compared with the pre-stimulus period in the corresponding frequency band. (*F–G*) Estimation of the interhemispheric asymmetry of the AER (7 babies). (*F*) Spatial positions of the probability for the channel to exhibit significant AER. (*G*) Total probability of detecting significant AER averaged over the principal channels (Cp5, T7, C3, FC5 for the left hemisphere and Cp6, T8, C4, FC6—for the right one). Note that AER was recorded more often in the right hemisphere than in the left one.

temporal area significant AER was detected with 0.5 ± 0.2 probability, compared to 0.75 ± 0.25 on the right (n = 7; Fig. 3G).

For spatial and temporal characterization of AERs, frequency decomposition was performed (Fig. 4A, B). However, because of low signal-to-noise ratio, AER characterization was mainly based on the peristimulus time histogram of the wavelet coefficients (Fig. 4B). Despite a wide distribution of significant oscillatory responses in delta, alpha, beta and gamma frequency ranges (Fig. 4C), the regions showing most oscillatory events were localized in the temporal lobe (Fig. 4C upper row). This was confirmed by the number of significant oscillatory events across all EEG channels: largest numbers were recorded on electrodes above the temporal lobe (Fig. 4C lower row). Analyzing spatial AERs distribution and significant wavelet coefficients of the models oscillations enabled picking the principal channels associated with the most powerful evoked cortical signals: Cp5, 6; T7, 8; C3, 4; FC5, 6. Further analysis of AERs' temporal profiles on these electrodes showed that oscillatory responses largely overlapped each other and occurred during the first part of long-lasting EEG deflection (Fig. 4D, E, Supplementary Fig. 3).

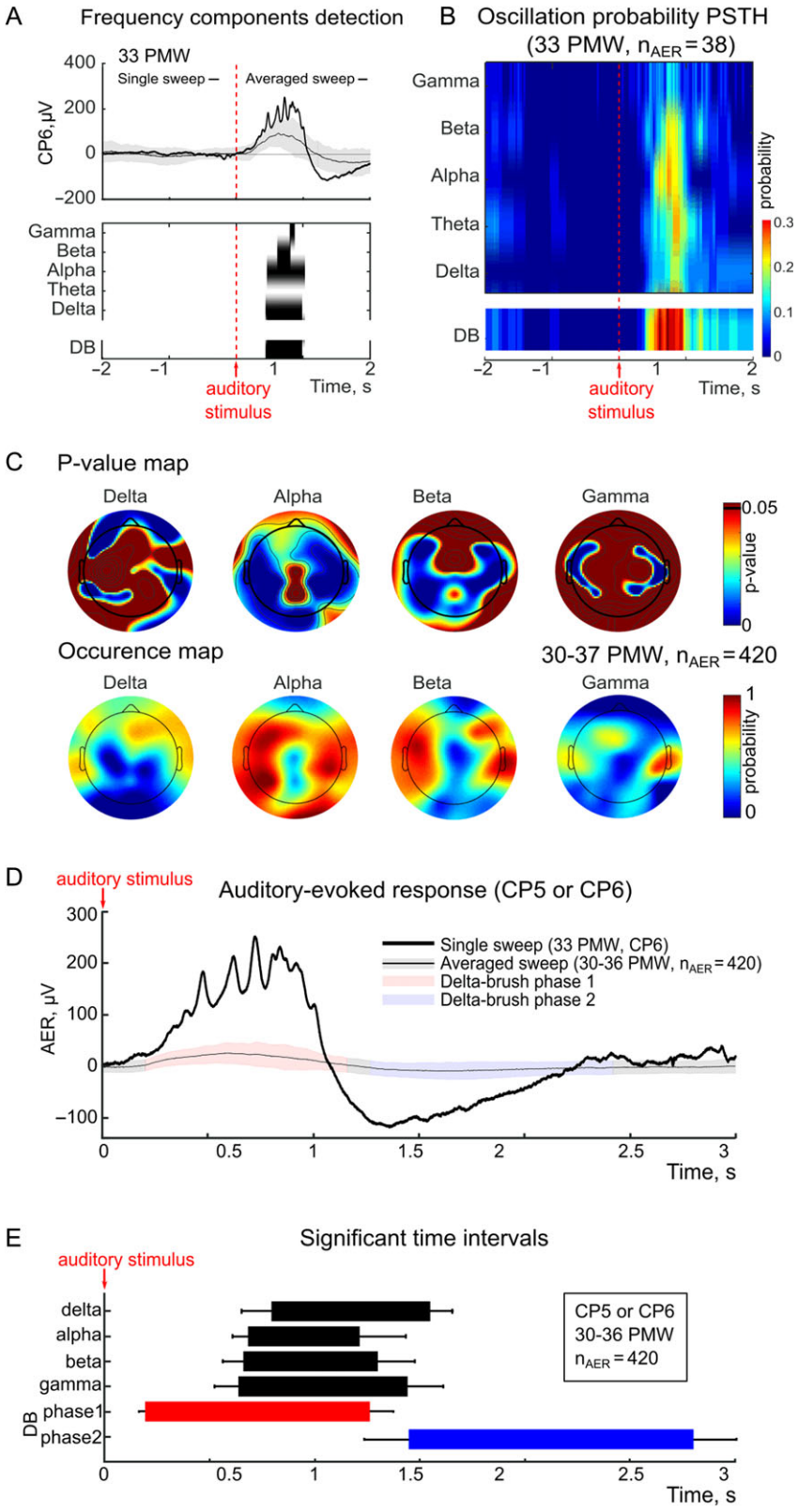

Figure 4. Temporal and spatial localization of the reconstructed oscillations of the AER. (*A*) Single AER (thick black line) overlaid on the averaged AERs (thin black line with shaded area corresponding to the STD) triggered by the auditory stimulus, recorded from the principal CP6 electrode (up) and temporal stamps of the reconstructed oscillatory components of this AER (down). (*B*) Peristimulus time histogram of the probability of the oscillatory events in the frequency ranges of interest during 4 s period triggered by the auditory stimulus (statistic is done based on 38 sweeps of premature of 33 PMW). Dash red line corresponds to the moment of the auditory stimulus; Note: 'DB' is the 'delta brush'. (*C*) *P*-value (up) and occurrence (down) maps of the auditory-evoked oscillatory responses of the frequency ranges of interest over the baby head. (*D*) Example of an AER overlaid on the averaged AER. The shaded area represents the standard deviation of AERs. Blue and red regions

Cortical Auditory-Evoked Potentials

Analysis was performed using 0.16 Hz high-pass filter and mean reference. Among the EEG recordings of the 30 infants, CAEPs evoked by click were identified in 24 (80%) subjects (Supplementay Table 1). They were 10/10 in Group 1, 5/8 in Group 2, and 9/12 in Group 3 (Supplementary Table 3). CAEPs were mostly found (1) when the number of stimuli exceeded 20 and (2) in QS rather than in AS ($P = 0.072$; Fisher's Exact Test) (Supplementary Table 1).

In Group 1: CAEPs occurred within 2000 ms after the stimulus and was composed of successive distinct negative slow waves (N1) identifiable on FC5-6, T7-8, and CP5-6 electrodes (Fig.5A). CP5-6 negative peak was followed by a huge late positivity peaking at around 1500 ms and lasting around 1 second (Fig. 5*A, B*; Supplementary Fig. 4Aa). The latencies of the negative peaks increased from FC5-6 to T7-8 and CP5-6 positions from 332 ms (+89) to 551 ms (+121) and 744 ms (+102), respectively ($P < 0.05$) (see Supplementary Fig. 4Aa, Supplementary Table 3). The amplitude of the CP5-6 peaks was higher than that of the FC5-6 peaks, 34 ± 16 μV and 20 ± 15 ($P < 0.05$), respectively (Fig. 5A, Supplementary Table 3, Supplementary Fig. 4Aa). Concomitantly to the FC5-6 negative peak, a positive peak was identifiable on PO7-8, O1-2, and P9-10 electrodes (Fig. 5*A, B*; Supplementary Fig. 4Aa). The CP5-6 negative peak was also concomitant to a positive slow wave (P2) on the midline CZ, FCZ electrodes with similar latency ($P > 0.05$) (Fig. 5*A, B*; Supplementary Fig. 4Aa). The CAEP consisted therefore of at least 2 successive dipoles with a negative pole on FC5-6 and then on CP5-6, and a positive pole on the posterior and then the anterior midline electrodes (Fig. 5*A,B*; Supplementry Table 3, Supplementary Fig. 4Aa).

In Group 3: the overall morphology of CAEP was similar to that of the younger Group 1 (Fig. 5*C*). An additional midline negative peak was identifiable in 2 neonates at a mean latency of 170 ± 33 ms (see Supplementary Fig. 4*Ba*). The latency of the P2 midline peak decreased between 30–33 and 37–38 PMW ($P < 0.05$), whereas the latencies of the T7-8, CP5-6, and FC5-6 peaks did not (Supplementary Table 3). These peak amplitudes remained unchanged between 30–33 and 36–38 PMW age.

We estimated the propagation speed of the negative slow wave (N1) around 13–14 cm/s from T7-8 to CP5-6 and around 11–12 cm/s from FC5-6 to T7-8 in group 1; and 10–12.5 cm/s and 16–17 cm/sin Group 3 respectively (Fig. 5*D*).

In Group 2: only 4/8 infants had identifiable CAEP, and there was no difference with the 2 previous groups (Supplementary Table 1).

The comparison between these CAEP data obtained using 0.16 Hz high-pass filter and mean reference and those obtained using 1.59 Hz high-pass filter and P reference is provided in Supplementary Material 2, Supplementary Table 3, and Supplementary Fig. 4.

Discussion

Previous studies with classical neonatal 9 electrodes setup showed that DBs can be evoked in a somatotopic manner in sensory cortices, depending on sensory modality (Milh et al. 2007; Colonnese et al. 2010; Chipaux et al. 2013). Using higher resolution EEG recordings and satisfactory localisation of electrodes with regards to underlying brain structures, this study details the spatio-temporal characteristics of cortical AERs in preterm neonates between 30 and 38 PMW: (1) there was an increase in EEG power from delta to gamma frequency bands (gamma is detected here for the first time as a part of sensory-evoked response in preterm neonates), over the middle and posterior temporal regions and predominating on the right hemisphere and during QS; (2) the slow (delta) component is superimposed with the fast (alpha–gamma) oscillatory component, both sharing the typical characteristics of DBs; (3) the slow component, which negatively peaks around 550 and 750 ms over the middle and posterior temporal regions respectively, corresponds to the late part of the CAEP, a feature to be missed with classical CAEP processing, due to (1) common lack of temporal site and long latency recording, (2) trial averaging masking oscillatory component, and (3) distortion by high-pass filtering and mastoid reference. In addition, the delta to alpha frequency bands power of this late component decreases until full term suggesting its link with the prenatal development of auditory processing circuits.

Auditory-Evoked DBs Detection

Evoked DBs rate in temporal regions varied with both age and vigilance state. Most babies aged 30–33 PMW had auditory-evoked DBs in QS identifiable both by visual and frequency power analyses, this response decreasing near term. This is in accordance with previous studies in visual and auditory-evoked DBs showing their progressive disappearance after 36 WPM (Colonnese et al. 2010: Chipaux et al. 2013). One limitation of the present study was the high variability of the number of stimuli among babies. Individual and environmental conditions being highly variable in this population lasting sleep was not easy to reach for some subjects. This limitation could specifically induce a bias in the inter-group analysis. We therefore analyzed a similar number of stimuli within the 3 age groups, selecting all those performed at the beginning of the recording, thus mostly in AS (since neonates fall asleep in AS). We found that AERs had a higher power increase in QS as previously reported, and our results suggest that at least 20 auditory stimulations are required to easily identify AERs (Weitzman et al. 1967; Rotteveel et al. 1987a, 1987b; Chipaux et al. 2013).

Regarding the number of required stimuli, our results are not surprising in line with classical principles of sensory-evoked responses analysis techniques, which require averaging repeated trials. In our study, spectral analysis of AERs provides a more objective tool than visual count of evoked temporal DBs; this kind of analysis, using grand-average, has been previously successfully performed in infants and adults, showing delta to gamma components and suggesting that cortical AER waves arise from the summation of spectral-temporal dynamics of EEG oscillations (Lippé et al. 2009; Ortiz-Mantilla et al. 2013; Musacchia et al. 2015). Here, spectral analysis shows significant increase of power spectrum at temporal electrodes in at least 3 frequency bands in 80% of the youngest infants (<34 PMW), suggesting it is also useful to study cortical AERs in preterm neonates.

represent up- and downwardly directed deflections of EEG, called phases 1 and 2, respectively. **E**: The on-, offsets, and durations of the reconstructed oscillatory components of the AER in the frequency ranges of interest are shown (used electrodes are Cp5, 6; T7,8; C3,4; FC5,6, $n = 7$ immature human babies). Note that the reconstructed oscillations are located predominantly by the end of the first phase of evoked DB. Group statistic was done based on 7 recordings with series of AER: at 30 PMW ($N = 92$ and $N = 58$), at 32 PMW ($N = 98$), at 33 PMW ($N = 73$ and 68), at 36 PMW ($N = 19$), and at 37 PMW ($N = 12$).

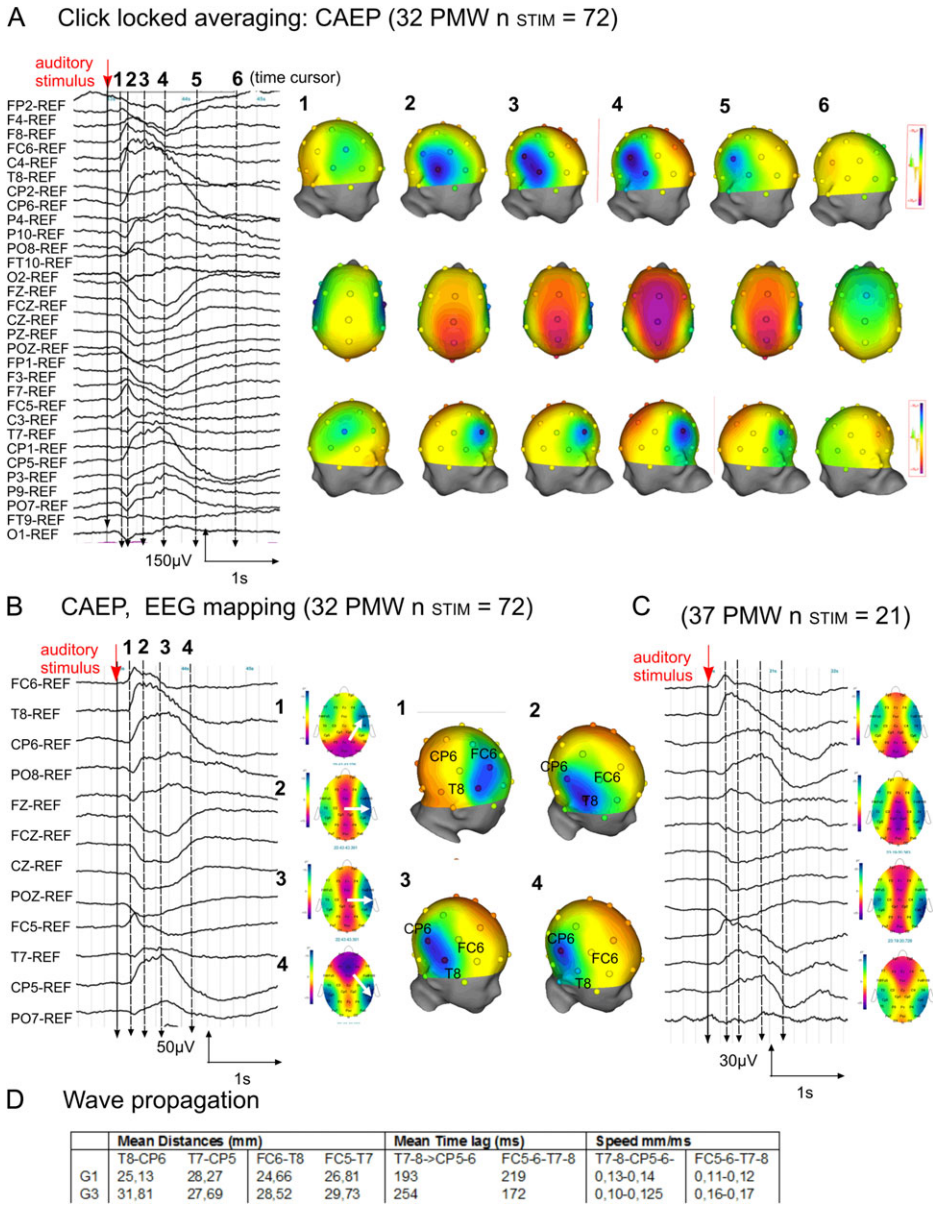

	Mean Distances (mm)				Mean Time lag (ms)		Speed mm/ms	
	T8-CP6	T7-CP5	FC6-T8	FC5-T7	T7-8->CP5-6	FC5-6-T7-8	T7-8-CP5-6-	FC5-6-T7-8
G1	25,13	28,27	24,66	26,81	193	219	0,13-0,14	0,11-0,12
G3	31,81	27,69	28,52	29,73	254	172	0,10-0,125	0,16-0,17

Figure 5. Click locked averaging: CAEP. (*A*) Example of CAEP in a 32 PMW neonate (averaging of 72 auditory stimuli "clicks"). On the left CAEP is represented on 31 EEG electrodes using 0.16 Hz high-pass filter and mean reference(upward deflection represents negative potential). On the right CAEP is represented on 3D EEG mapping (coherence software Mapping 3D adapted for present research), locked to the positions as defined by the time cursor (dashed lines): at the beginning of the negative wave (1), at the 3 successive negative peaks on FC5-6 (2), T7-8 (3), and CP5-6 (4), at the end of the negative peak on CP5-6 (5) and at the CP5-6 positive peak (6). Note, the positivity at the vertex(seen from up high) concomitant to the negative peaks. (*B*) Zoom on CAEP in 32 and 37 PMW neonates: On the left CAEP is represented on 13 electrodes of interest and on the middle, CAEP is represented on 2D mapping locked at the time as defined by the cursor (dashed lines): at 3 successive negative peaks on FC5-6 (1), T7-8 (2), and CP5-6 (3) electrodes and at the end of the negative peak on CP5-6 (4). Note, the positive peaks on the midline concomitant with the negative lateral peaks, and the dipole reversal moving caudo-rostrally. On the right: CAEP is represented on 3D mapping locked to the position as defined by the time cursor. (*C*) Example of CAEP in a 37 PMW neonate represented on 13 EEG electrodes and on 2D mapping as above. (*D*) Propagation speed of the evoked waves betweenT7-8 and CP5-6 and between FC5-6 and T7-8 electrodes.

Network Mechanisms of the Auditory-evoked DBs

The mechanisms involved in the generation of spontaneous and sensory-evoked DBs in preterm infants remain largely hypothetical so far. One hypothesis involves the transient circuits in the fetal cortex, notably the subplate that shows a developmental profile remarkably similar to the bell-shaped developmental profile of DBs whose occurrence increases from 28 PMW to 32–34 PMW and decreases afterwards so that DBs disappear near term (Kostović and Judas 2006, 2010; André et al. 2010; Kanold and Luhmann 2010; Hoerder-Suabedissen and Molnar 2015). The "subplate stage" in humans covers the 15–35 PMW period, while the subplate expansion is partly due to the invasion by various in-growing fibers (thalamo-cortical afferents, basal forebrain cholinergic, callosal, and ipsilateral cortico-cortical afferents). The subplate zone represents therefore a dynamic "waiting compartment" playing a critical role in the establishment of intracortical and extra-cortical circuitries, and guiding the thalamic inputs to the topographically aligned

cortical loci (Kostovic and Rakic 1990; Hoerder-Suabedissen and Molnar 2015). This local network has been proposed to act as an amplifier of thalamic and neuromodulatory input coordinating activity and regulating ocular-dominance plasticity (Kanold and Shatz 2006; Luhmann et al. 2009) well as early rhythmic activity (Dupont et al. 2006; Tolner et al. 2012). Consistent with this hypothesis, the ablation of the subplate severely impairs spindle-bursts in the somatosensory cortex of neonatal rodents (Tolner et al. 2012). Electrophysiological recordings from individual cells in acute postmortem brain slices from human fetal cerebral cortex showed that human subplate neurons (SPn) are spontaneously active as early as 16–22 PMW: they display bursts of electrical activity consisting of sustained plateau depolarizations and bursts of action potential firing with the peak frequencies of 40–60 Hz comparable to those reported in early postnatal SPn in rodents (Luhmann et al. 2009; Moore et al. 2009, 2011, 2014). This pattern resembled the "trace discontinu" in EEG recordings from preterm infants, thus supporting the hypothesis that SPn-thalamo-cortical afferents networks might be involved in the generation of the DBs pattern (Moore et al. 2009, 2011, 2014; André et al. 2010). The 'subplate dissolution' stage occurs in humans at >35 PMW, when SPn decline in number and the volume of subplate decreases. This stage is concurrent with the secondary gyrification of the brain. In addition to the subplate, other transient circuits may be involved in the generation of transitory EEG patterns, such as the dense but transient innervation of infragranular somatostatin interneurons by thalamocortical afferents that appears to be essential for the development of feedforward inhibition in rodent's somatosensory cortex (Marques-Smith et al. 2016; Tuncdemir et al. 2016). Also, the delayed maturation of inhibitory mechanisms due to delayed maturation of potassium chloride co-transporter 2 (KCC2) and elevated expression of potassium chloride co-transporter1 (NKCC1) in the immature cortical neurons has been shown to be correlated with the expression of DBs and SATs in the visual cortex (Dzhala et al. 2005; Vanhatalo et al. 2005).

Studies in animal models have also provided some insights into DBs' underlying mechanisms. During postnatal days P0-12 in rodents, a developmental period corresponding to the second half of human gestation, cortical sensory (sensorimotor and visual) areas display discontinuous temporal organization and characteristic activity patterns, such as early gamma and SBs oscillations and SATs in the visual cortex, that share many common features with human preterm DBs (Clancy et al. 2001, 2007; Khazipov and Luhmann 2006; Colonnese et al. 2010; Colonnese and Khazipov 2012; Khazipov et al. 2013; Workman et al. 2013; Luhmann et al. 2016; see also http://www.translatingtime.net/). Despite the lack of direct experimental demonstration, spontaneous cochlear bursts might also trigger SBs in the immature auditory cortex, and drive bursts of activity in subcortical auditory stations (Tritsch et al. 2007, 2010; Wang et al. 2015). This raises the hypothesis that "spontaneous" DBs in human auditory cortex might be driven by spontaneous cochlear bursts. Nevertheless, human fetuses and preterm neonates strongly differ from neonatal rodents in the early responsiveness of the auditory system, present from the onset of thalamo-cortical development in humans, contrarily to rodents that are deaf until the second postnatal week (Chang and Merzenich 2003). The reasons of this interspecies' difference are unknown: a delayed physical development of the auditory periphery might be involved, protecting from external stimuli that would otherwise interfere with cochlear bursts in driving the auditory system construction. By analogy to visual and somatosensory evoked potentials, the initial CAEP component is most likely generated by direct transmission of excitation through the auditory pathways. These initial CAEP responses have longer latencies in neonates than in adults, reflecting the low pathways myelination. The late component of CAEP, that is, the DB per se, likely involves thalamic bursts organized in fast oscillations (including gamma rhythmic activity) (Minlebaev et al. 2011; Yang et al. 2013), as well as intracortical processing and cortico-thalamic feedback (generating larger scale patterning at alpha–beta frequencies) (Contreras et al. 1996a; Dupont et al. 2006; Minlebaev et al. 2007; Yang et al. 2013; Murata and Colonnese 2016).

The present study is the first to detect gamma oscillations as a part of AER in human preterm neonates although they were previously reported during spontaneous activity in preterm infants, visual evoked responses in term neonates, and AERs in toddlers (Milh et al. 2007; Grieve et al. 2008; Isler et al. 2007; Musacchia et al. 2015). Gamma oscillations are also observed in the adult brain during AERs (Galambos et al. 1981). The EGOs that we report here display some particular features. First, they occur with a remarkable delay after the stimulus beginning nearly at the peak of delta wave whereas in neonatal rats, EGOs are primarily driven by rhythmic gamma excitation from the thalamus and occurs at the beginning of the SBs, (Minlebaev et al. 2011; An et al. 2012, 2014; Khazipov et al. 2013; Yang et al. 2013). Second, their mechanisms are likely very different from adults. Indeed, adults gamma oscillations are generated by synchronous perisomatic inhibition mechanism (Buzsaki and Wang 2012), whereas in neonatal rats, EGOs are primarily generated by the gamma rhythmic input from thalamus with a delayed recruitment of the perisomatic inhibition (Daw et al. 2007; Minlebaev et al. 2011; Yang et al. 2013).

As shown in neonatal rodent visual and somatosensory cortices, the delta component of SBs results from temporal summation of the excitatory synaptic currents with a notable contribution of NMDA receptors. This component nests rapid oscillations and its magnitude correlates positively with neuronal depolarization, firing and the power of fast oscillations (Minlebaev et al. 2007; Colonnese and Khazipov 2010). Therefore, delta waves as a DB component are mechanistically different from adult delta waves, which are associated with a collective cessation of neuronal activity (up to down state transition) for a period of up to a few hundred milliseconds during slow wave sleep or quiet wakefulness (Contreras et al. 1996b; Sanchez-Vives and McCormick 2000). Adult delta waves also curtail the early sensory-evoked responses, and are followed by the rebound up-states with fast oscillations during sleep or quiet wake states and under anesthesia, together forming characteristic K-complexes. Thus, the only similarity between the preterm DBs and adult delta waves consists of their electrographic appearance, while underlying mechanisms are cardinally different. This stresses the necessary caution in interpreting EEG grapho-elements in preterm neonates only on the basis of their electrographic appearance.

Auditory-Evoked DB is the Slow Temporal Component of CAEP Traveling Through Temporal Regions

The latency and morphology of CAEP peaks substantially changed when using high-pass filtering as low as possible and mean reference, compared to the classic filtering and mastoid reference (Supplementary Material 2 and Supplementary Fig. 3; Rotteveel et al., 1987a, 1987b). We also identified a late, long-lasting, and not previously reported positivity at 1500 ms on CP5-CP6 electrodes. Reanalyzing our data at 30–33 PMW with a set-up similar to normative studies of CAEP in premature

infants of the same age range (1.59 Hz high-pass filter, P reference, see details in Supplementary Material 2) (Weitzman et al. 1967; Rotteveel et al. 1987a, 1987b; Wunderlich and Cone-Wesson 2006), we found a FC5-6 negative peak at a latency similar to the previously reported "lateral negativity" (237 ± 21 ms) and 2 other negative T7-8 and CP5-–6 waves at 254 ± 16 and 275 ± 38 ms, respectively. These late components had not been previously reported in normative studies due to lack of temporal site recordings. Modifying filtering and reference schemes are known to result in dramatic effects on ERP signals (Widmann et al. 2015). Not surprisingly we did observe major differences in CAEP components between the classical setting and the present one: (1) peak amplitude was lower, and T7-8 and CP5-6 slow waves were either distorted or suppressed, (2) peak latency became shorter, (3) mastoid reference also induced changes in the global morphology of CAEP peaks, the negative peaks becoming diffuse likely due to an active potential on the mastoid. As a result, temporal DBs proved to correspond to the negative slow wave recorded at T7-8 and CP5-6 electrodes and thus to the late negative component of CAEPs.

Using MEG, the sources of the 250-ms CAEP response have been successfully localized in the auditory cortex in fetuses aged 29–36 PMW (Lengle et al. 2001) and in newborns (Huotilainen et al. 2003; Sambeth et al. 2009) suggesting that the auditory-evoked DBs do originate in the auditory cortices (at least the T7-8 slow wave that occurs at 254 ± 16 ms with the classical high-pass filtering). Noteworthy, a late and slow component with large negative amplitude (identified here as evoked DB) has also been observed as the main response in visual and somatosensory-evoked potentials before 35 PMW, progressively disappearing with age (Hrbek et al. 1973). Thus, this slow component might be a hallmark of immature evoked potentials, that is, of immature cortical sensory processing, whatever the sensory modality (Khazipov and Luhman 2006; Milh et al. 2007; Colonnese et al. 2010; Chipaux et al. 2013).

The clicks used in the present study are broadband sounds exciting all parts of the basilar membrane, resulting in tonotopic activation from higher to lower frequencies (Robles and Ruggero 2001). In adults, frequency gradients in auditory cortex progress along 2, roughly orthogonal axes: anterior–posterior parallel to supra-temporal gyrus and medial to lateral in supra-temporal plane along Heschl's gyrus (Leaver and Rauschecker 2016). EEG mapping of the CAEP with our electrodes localisation disclosed at least 2 waves with the negative potential successively at FC5-6, T7-T8, and CP5-6, and with polarity reversal moving caudo-rostrally, thus possibly reflecting activation of tonotopic maps. Interestingly we found that the negative slow component of the AER, that is, the evoked DB, propagates from T7-8 to CP5-6 with an estimated speed of 10–14 cm/s, in line with the speed of previously reported travelling waves in human motor and sensory cortices as well as in rat auditory cortex (Reimer et al. 2011; Takahashi et al. 2011; Sato et al. 2012). In the auditory cortex of adult rats, responses evoked after a broad band click consist of waves travelling from the primary auditory anterior fields to higher-order fields, suggesting the integration of in-coming acoustic information over the whole auditory cortex in the form of a propagating wave (Reimer et al. 2011).

However, our study has several limitations hampering accurate electric current dipole localization. Indeed, by contrast with MEG that provides accurate source reconstruction, EEG source localization is more challenging in premature infants. Realistic neonatal head models are still lacking due to uncertainty in head tissue conductivities and geometrical complexities including fontanels (Wolters et al. 2006; Odabaee et al. 2014; Azizollahi et al. 2016). We used "only" 32 electrodes placed according to the classical 10–10 international system, whatever age and head size. Recent studies have shown that neonatal/infant scalp EEG has a very high spatial content resulting from high skull conductivity and decay within few centimetres at the scalp (i.e.the 12–20 Hz band spatial regions change from their peak value to the noise floor in approximatively 40 mm) (Grieve et al. 2004; Odabaee et al. 2013, 2014). Determining the optimal number and spacing of EEG electrodes depends on the spatial variation of electrical potential (spatial Nyquist sampling rate). Our 32 electrodes caps enabled to reach a between-electrode distance of 20–25 mm in the youngest infants, which is considered acceptable with regard to the spatial frequency of DB delta-alpha band components (Odabaee et al. 2013), but was probably insufficient to more accurately study the spatio-temporal dynamics of the gamma components of AERs. Moreover, we could not register the electrodes position on the infant's own MRI, as MRI examination could not be obtained in this study. While it was beyond the scope of this article to describe extensively electrode localizations as proposed in infants (Kabdebon et al. 2014), our MRI template-based approach allowed us to highlight the negligible topographic variability across the 3 age groups of the electrodes showing AERs.

A Right Hemisphere Predominance of Auditory DBs Evoked by Click Stimuli

The rightward asymmetry we observed in the present study may be explained by 2 processes, maturation and specialization, that probably occur in parallel throughout human brain development. First, brain maturation is earlier in the right than in the left hemisphere: (1) during the third trimester of gestation, gyral complexity of the superior temporal sulcus develops earlier on the right side (Chi et al. 1977; Dubois et al. 2010); (2) cerebral blood flow at rest is higher in the right hemisphere from 1 to 3 years of age, before the asymmetry starts to shift to the left (Chiron et al. 1997; Lin et al. 2013); (3) EEG power spectrum below 13 Hz at rest is also higher in the right hemisphere between 35 and 45 weeks of gestation (Myers et al. 2012); (4) the right hemisphere shows higher genetic expression levels than the left during gestation (Sun and Walsh 2006).

Besides, there is an early emerging hemispheric specialization for auditory processing. CAEP disclose functional asymmetry as early as 35 PMW, with higher activity on the right than on the left temporal electrodes for both tones detection and discrimination (Mento et al. 2010). Interestingly, the corresponding evoked responses occur selectively between 350 and 650 ms after the stimulus, that is, within the time window we characterized as the "late negative response" (Mento et al. 2010). On the other hand, the left temporal regions seem rather dedicated to process the specific properties of speech, as shown at birth using optical topography (Peña et al. 2003; Mahmoudzadeh et al. 2013) and at 3 months using functional MRI (Dehaene-Lambertz et al. 2006). From the last trimester of gestation on, the sylvian fissure is larger on the left side, close to Broca's region and planum temporale, suggesting the early emergence of functional lateralization for language processing (Chi et al. 1977; Dehaene-Lambertz et al. 2006; Dubois et al. 2008a, 2008b, 2010). While an early specialization of perisylvian regions exists for speech sounds, it might also be the case for nonlinguistic sounds like tones or clicks. In adults, there is strong evidence that spectral information mainly involves the right primary auditory field whereas temporal information is dominantly processed in the left field (Belin et al. 2002; Zatorre et al. 2002; Woods et al. 2011; Cha et al. 2016).

Conclusion

In premature neonates, auditory-evoked "DBs" contain broad band responses ranging from delta to gamma frequencies that originate from the temporal cortex. Together with previous data from animals and humans, our results suggest that sensory-evoked DBs are part of sensory-evoked potentials and that early gamma activity contributes to the formation of sensory maps (Minlebaev et al. 2011; Yang et al.2013). From this perspective we can hypothesize that over-stimulation with inappropriate stimuli, whatever the sensory modality, could have deleterious effects on sensory cortices maturation of prematurely born infants. Present findings also raise the question whether sensory-evoked DBs might be seen as a functional test for sensory cortices in premature infants. High resolution EEG studies with increased number of electrodes and source modelling are needed for further delineation of spatio-temporal dynamics of sensory-evoked DBs.

Supplementary Material

Supplementary data are available at *Cerebral Cortex* online.

Funding

The French National Research Agency (ANR-09-MNPS-006 "Delta-Brushes" Early Activity in the Immature Brain).

Notes

We thank Pr Petra Hüppi (from Geneva University Hospitals) for providing the preterm MRI data. We thank Daniele Decarpentry and Maurice Lemeux for recording the infants and Walter Janssens and Laurent Fousseret (Deltamed/Natus France) for technical assistance and software adaptation for the purpose of this research project. We thank Pr Olivier Dulac for his advice on the manuscript. *Conflict of Interest*: None declared.

References

Guideline 9C. 2008. guidelines on short-latency auditory evoked potentials. American Clinical Neurophysiology Society. Am J Electroneurodiagnostic Technol. 46:275–286.

Acunzo DJ, Mackenzie G, van Rossum MC. 2012. Systematic biases in early ERP and ERF components as a result of high-pass filtering. J Neurosci Methods. 209:212–218.

An S, Yang JW, Sun H, Kilb W, Luhmann HJ. 2012. Long-term potentiation in the neonatal rat barrel cortex in vivo. J Neurosci. 32:9511–9516.

An S, Kilb W, Luhmann HJ. 2014. Sensory-evoked and spontaneous gamma and spindle bursts in neonatal rat motor cortex. J Neurosci. 34:10870–10883.

André M, Lamblin MD, d'Allest AM, Curzi-Dascalova L, Moussalli-Salefranque F, Nguyen S, Vecchierini-Blineau MF, Wallois F, Walls-Esquivel E, Plouin P. 2010. Electroencephalography in premature and full-term infants. Developmental features and glossary. Neurophysiol Clin. 40:59–124.

Azizollahi H, Aarabi A, Wallois F. 2016. Effects of uncertainty in head tissue conductivity and complexity on EEG forward modeling in neonates. Hum Brain Mapp. 37:3604–3622.

Belin P, Zatorre RJ, Ahad P. 2002. Human temporal-lobe response to vocal sounds. Brain Res Cogn Brain Res. 13:17–26.

Buzsaki G, Wang XJ. 2012. Mechanisms of gamma oscillations. Annu Rev Neurosci. 35:203–225.

Cha K, Zatorre RJ, Schönwiesner M. 2016. Frequency selectivity of voxel-by-voxel functional connectivity in human auditory cortex. Cereb Cortex. 26:211–224.

Chang EF, Merzenich MM. 2003. Environmental noise retards auditory cortical development. Science. 300:498–502.

Chi JG, Dooling EC, Gilles FH. 1977. Left-right asymmetries of the temporal speech areas of the human fetus. Arch Neurol. 34:346–348.

Chipaux M, Colonnese MT, Mauguen A, Fellous L, Mokhtari M, Lezcano O, Milh M, Dulac O, Chiron C, Khazipov R, et al. 2013. Auditory stimuli mimicking ambient sounds drive temporal "delta-brushes" in premature infants. PLoS One. 8:e79028.

Chiron C, Jambaque I, Nabbout R, Lounes R, Syrota A, Dulac O. 1997. The right brain hemisphere is dominant in human infants. Brain. 120:1057–1065.

Clancy B, Darlington RB, Finlay BL. 2001. Translating developmental time across mammalian species. Neuroscience. 105: 7–17.

Clancy B, Finlay BL, Darlington RB, Anand KJ. 2007. Extrapolating brain development from experimental species to humans. Neurotoxicology. 28:931–937.

Colonnese MT, Kaminska A, Minlebaev M, Milh M, Bloem B, Lescure S, Moriette G, Chiron C, Ben-Ari Y, Khazipov R. 2010. A conserved switch in sensory processing prepares developing neocortex for vision. Neuron. 67:480–498.

Colonnese MT, Khazipov R. 2010. "Slow activity transients" in infant rat visual cortex: a spreading synchronous oscillation patterned by retinal waves. J Neurosci. 30:4325–4337.

Colonnese M, Khazipov R. 2012. Spontaneous activity in developing sensory circuits: Implications for resting state fMRI. Neuroimage. 62:2212–2221.

Contreras D, Destexhe A, Sejnowski TJ, Steriade M. 1996a. Control of spatiotemporal coherence of a thalamic oscillation by corticothalamic feedback. Science. 274:771–774.

Contreras D, Timofeev I, Steriade M. 1996b. Mechanisms of long-lasting hyperpolarizations underlying slow sleep oscillations in cat corticothalamic networks. J Physiol. 494:251–264.

Curzi-Dascalova L, Figueroa JM, Eiselt M, Christova E, Virassamy A, d'Allest AM, Guimarâes H, Gaultier C, Dehan M. 1993. Sleep state organization in premature infants of less than 35 weeks' gestational age. Pediatr Res. 34:624–628.

Daw MI, Ashby MC, Isaac JT. 2007. Coordinated developmental recruitment of latent fast spiking interneurons in layer IV barrel cortex. Nat Neurosci. 10:453–461.

Dehaene-Lambertz G, Hertz-Pannier L, Dubois J. 2006. Nature and nurture in language acquisition: anatomical and functional brain-imaging studies in infants. Trends Neurosci. 2: 367–373.

Delorme A, Makeig S. 2004. EEGLAB: an open source toolbox for analysis of single-trial EEG dynamics including independent component analysis. J Neurosci Methods. 134:9–21.

Desmedt JE, Manil J. 1970. Somatosensory evoked potentials of the normal human neonate in REM sleep, in slow wave sleep and in waking. Electroencephalogr Clin Neurophysiol. 29:113–126.

Dubois J, Benders M, Cachia A, Lazeyras F, Ha-VinhLeuchter R, Sizonenko SV, Borradori-Tolsa C, Mangin JF, Hüppi PS. 2008a. Mapping the early cortical folding process in the preterm newborn brain. Cereb Cortex. 18:1444–1454.

Dubois J, Benders M, Borradori-Tolsa C, Cachia A, Lazeyras F, Ha-VinhLeuchter R, Sizonenko SV, Warfield SK, Mangin JF, Hüppi PS. 2008b. Primary cortical folding in the human newborn: an early marker of later functional development. Brain. 131:2028–2041.

Dubois J, Benders M, Lazeyras F, Borradori-Tolsa C, Leuchter RH, Mangin JF, Hüppi PS. 2010. Structural asymmetries of perisylvian regions in the preterm newborn. Neuroimage. 52:32–42.

Dupont E, Hanganu I, Kilb W, Hirsch S, Luhmann HJ. 2006. Rapid developmental switch in the mechanisms driving early cortical columnar networks. Nature. 439:79–83.

Dzhala VI, Talos DM, Sdrulla DA, Brumback AC, Mathews GC, Benke TA, Delpire E, Jensen FE, Staley KJ. 2005. NKCC1 transporter facilitates seizures in the developing brain. NatMed. 11:1205–1213.

Fabrizi L, Worley A, Patten D, Holdridge S, Cornelissen L, Meek J, Boyd S, Slater R. 2011. Electrophysiological measurements and analysis of nociception in human infants. J Vis Exp. 20:pii3118.

Galambos R, Makeig S, Talmachoff PJ. 1981. A 40-Hz auditory potential recorded from the human scalp. Proc Natl Acad Sci USA. 78:2643–2647.

Grieve PG, Isler JR, Izraelit A, Peterson BS, Fifer WP, Myers MM, Stark RI. 2008. EEG functional connectivity in term age extremely low birth weight infants. Clin Neurophysiol. Dec. 119:2712–2720.

Grieve PG, Emerson RG, Isler JR, Stark RI. 2004. Quantitative analysis of spatial sampling error in the infant and adult electroencephalogram. Neuroimage. 21(4):1260–1274.

Hanganu IL, Ben Ari Y, Khazipov R. 2006. Retinal waves trigger spindle bursts in the neonatal rat visual cortex. J Neurosci. 26:6728–6736.

Hanganu-Opatz IL. 2010. Between molecules and experience: role of early patterns of coordinated activity for the development of cortical maps and sensory abilities. Brain Res Rev. 64:160–176.

Hoerder-Suabedissen A, Molnar Z. 2015. Development, evolution and pathology of neocortical subplate neurons. Nat Rev Neurosci. 16:133–146.

Hrbek A, Karlberg P, Olsson T. 1973. Development of visual and somatosensory evoked responses in pre-term newborn infants. Electroencephalogr Clin Neurophysiol. 34:225–232.

Huotilainen M, Kujala A, Hotakainen M, Shestakova A, Kushnerenko E, Parkkonen L, Taulu S, Simola J, Nenonen J, Karjalainen M, et al. 2003. Auditory magnetic responses of healthy newborns. Neuroreport. 14:1871–1875.

Isler JR, Grose-Fifer J, Fifer WP, Housman S, Stark RI, Grieve PG. 2007. Frequency domain analyses of neonatal flash VEP. Pediatr Res. 62:581–585.

Kabdebon C, Leroy F, Simmonet H, Perrot M, Dubois J, Dehaene-Lambertz G. 2014. Anatomical correlations of the international 10–20 sensor placement system ininfants. Neuroimage. 99:342–356.

Kanold PO, Shatz CJ. 2006. Subplate neurons regulate maturation of cortical inhibition and outcome of ocular dominance plasticity. Neuron. 51(5):627–638.

Kanold PO, Luhmann HJ. 2010. The subplate and early cortical circuits. Annu Rev Neurosci. 33:23–48.

Khazipov R, Sirota A, Leinekugel X, Holmes G, Ben Ari Y, Buzsaki G. 2004. Early motor activity drives spindle bursts in the developing somatosensory cortex. Nature. 432:758–761.

Khazipov R, Luhmann HJ. 2006. Early patterns of electrical activity in the developing cerebral cortex of humans and rodents. Trends Neurosci. 29:414–418.

Khazipov R, Minlebaev M, Valeeva G. 2013. Early gamma oscillations. Neuroscience. 250:240–252.

Koolen N, Dereymaeker A, Rasanen O, Jansen K, Vervisch J, Matic V, De Vos M, Naulaers G, Van Huffel S, Vanhatalo S. 2015. Data-driven metric representing the maturation of preterm EEG. ConfProc IEEE Eng Med Biol Soc. 2015: 1492–1495.

Koolen N, Dereymaeker A, Räsänen O, Jansen K, Vervisch J, Matic V, Naulaers G, De Vos M, Van Huffel S, Vanhatalo S. 2016. Early development of synchrony in cortical activations in the human. Neuroscience. 322:298–307.

Kostovic I, Judas M. 2006. Prolonged coexistence of transient and permanent circuitry elements in the developing cerebral cortex of fetuses and preterm infants. Dev Med Child Neurol. 48:388–393.

Kostović I, Judas M. 2010. The development of the subplate and thalamocortical connections in the human foetal brain. Acta Paediatr. 99(8):1119–1127.

Kostovic I, Rakic P. 1990. Developmental history of the transient subplate zone in the visual and somatosensory cortex of the macaque monkey and human brain. J Comp Neurol. 297(3): 441–470.

Lamblin MD, André M, Challamel MJ, Curzi-Dascalova L, d'Allest AM, De Giovanni E, Moussalli-Salefranque F, Navelet Y, Plouin P, Radvanyi-Bouvet MF, et al. 1999. Electroencephalography of the premature and term newborn. Maturational aspects and glossary. Neurophysiol Clin. 29:123–219.

Leaver AM, Rauschecker JP. 2016. Functional topography of human auditory cortex. J Neurosci. 36:1416–1428.

Lengle JM, Chen M, Wakai RT. 2001. Improved neuromagnetic detection of fetal and neonatal auditory-evokedresponses. Clin Neurophysiol. 112:785–792.

Lin PY, Roche-Labarbe N, Dehaes M, Carp S, Fenoglio A, Barbieri B, Hagan K, Grant PE, Franceschini MA. 2013. Non-invasive optical measurement of cerebral metabolism and hemodynamics in infants. J Vis Exp. 73:e4379.

Lippé S, Martinez-Montes E, Arcand C, Lassonde M. 2009. Electrophysiological study of auditory development. Neuroscience. 164(3):1108–1118.

Luhmann HJ, Sinning A, Yang JW, Reyes-Puerta V, Stuttgen MC, Kirischuk S, Kilb W. 2016. Spontaneous neuronal activity in developing neocortical networks: from single cells to large-scale interactions. Front Neural Circuits. 10:40.

Luhmann HJ, Kilb W, Hanganu-Opatz IL. 2009. Subplate cells: amplifiers of neuronal activity in the developing cerebral cortex. Front Neuroanat. 3:19.

Mahmoudzadeh M, Dehaene-Lambertz G, Fournier M, Kongolo G, Goudjil S, Dubois J, Grebe R, Wallois F. 2013. Syllabic discrimination in premature human infants prior to complete formation of cortical layers. Proc Natl Acad Sci USA. 110: 4846–4851.

Marques-Smith A, Lyngholm D, Kaufmann AK, Stacey JA, Hoerder-Suabedissen A, Becker EB, Wilson MC, Molnár Z, Butt SJ. 2016. A transient translaminar GABAergic interneuron circuit connects thalamocortical recipient layers in neonatal somatosensory cortex. Neuron. 89:536–549.

Mento G, Suppiej A, Altoè G, Bisiacchi PS. 2010. Functional hemispheric asymmetries in humans: electrophysiological evidence from preterm infants. Eur J Neurosci. 31:565–574.

Milh M, Kaminska A, Huon C, Lapillonne A, Ben-Ari Y, Khazipov R. 2007. Rapid cortical oscillations and early motor activity in premature human neonate. Cereb Cortex. 17: 1582–1594.

Minlebaev M, Ben-Ari Y, Khazipov R. 2007. Network mechanisms of spindle-burst oscillations in the neonatal rat barrel cortex in vivo. J Neurophysiol. 97:692–700.

Minlebaev M, Colonnese M, Tsintsadze T, Sirota A, Khazipov R. 2011. Early gamma oscillations synchronize developing thalamus and cortex. Science. 334:226–229.

Moore AR, Filipovic R, Mo Z, Rasband MN, Zecevic N, Antic SD. 2009. Electrical excitability of early neurons in the human cerebral cortex during the second trimester of gestation. Cereb Cortex. 19(8):1795–1805.

Moore AR, Zhou WL, Jakovcevski I, Zecevic N, Antic SD. 2011. Spontaneous electrical activity in the human fetal cortex in vitro. J Neurosci. 31(7):2391–2398.

Moore AR, Zhou WL, Sirois CL, Belinsky GS, Zecevic N, Antic SD. 2014. Connexin hemichannels contribute to spontaneous electrical activity in the human fetal cortex. Proc Natl Acad Sci USA. 111(37):E3919–E3928.

Murata Y, Colonnese MT. 2016. An excitatory cortical feedback loop gates retinal wave transmission in rodent thalamus. Elife. 11:5.

Musacchia G, Ortiz-Mantilla S, Realpe-Bonilla T, Roesler CP, Benasich AA. 2015. Infant auditory processing and event-related brain oscillations. J Vis Exp. (101):e52420. doi: 10.3791/52420.

Myers MM, Grieve PG, Izraelit A, Fifer WP, Isler JR, Darnall RA, Stark RI. 2012. Developmental profiles of infant EEG: overlap with transient cortical circuits. ClinNeurophysiol. 123: 1502–1511.

Odabaee M, Freeman WJ, Colditz PB, Ramon C, Vanhatalo S. 2013. Spatial patterning of the neonatal EEG suggests a need for a high number of electrodes. Neuroimage. 68:229–235.

Odabaee M, Tokariev A, Layeghy S, Mesbah M, Colditz PB, Ramon C, Vanhatalo S. 2014. Neonatal EEG at scalp is focal and implies high skull conductivity in realistic neonatal head models. Neuroimage. 96:73–80.

Ortiz-Mantilla S, Hämäläinen JA, Musacchia G, Benasich AA. 2013. Enhancement of gamma oscillations indicates preferential processing of native over foreign phonemic contrasts in infants. J Neurosci. 33(48):18746–18754.

Peña M, Maki A, Kovacić D, Dehaene-Lambertz G, Koizumi H, Bouquet F, Mehler J. 2003. Sounds and silence: an optical topography study of language recognition at birth. Proc Natl Acad Sci USA. 100:11702–11705.

Picton TW, Alain C, Woods DL, John MS, Scherg M, Valdes-Sosa P, Bosch-Bayard J, Trujillo NJ. 1999. Intracerebral sources of human auditory-evoked potentials. AudiolNeurootol. 4: 64–79.

Qin Y, Xu P, Yao DA. 2010. Comparative study of different references for EEG default mode network: the use of the infinity reference. Clin Neurophysiol. 121:1981–1991.

Reimer A, Hubka P, Engel AK, Kral A. 2011. Fast propagating waves within the rodent auditory cortex. Cereb Cortex. 21(1):166–177.

Robles L, Ruggero MA. 2001. Mechanics of the mammalian cochlea. Physiol Rev. 81(3):1305–1352.

Rotteveel JJ, Colon EJ, Stegeman DF, Visco YM. 1987a. The maturation of the central auditory conduction in preterm infants until 3 months post term IV. Composite group averages of the cortical auditory-evokedresponses (ACRs). Hearing Res. 27:85–93.

Rotteveel JJ, Colon EJ, Stegeman DF, Visco YM. 1987b. The maturation of the central auditory conduction in preterm infants until 3 months post term V. The auditory cortical response (ACR). Hearing Res. 27:95–100.

Sambeth A, Pakarinen S, Ruohio K, Fellman V, van Zuijen TL, Huotilainen M. 2009. Change detection in newborns using a multiple deviant paradigm: a study using magnetoencephalography. Clin Neurophysiol. 120:530–538.

Sanchez-Vives MV, McCormick DA. 2000. Cellular and network mechanisms of rhythmic recurrent activity in neocortex. Nat Neurosci. 3:1027–1034.

Sato TK, Nauhaus I, Carandini M. 2012. Traveling waves in visual cortex. Neuron. 75:218–229.

Stjerna S, Voipio J, Metsäranta M, Kaila K, Vanhatalo S. 2012. Preterm EEG: a multimodal neurophysiological protocol. J Vis Exp. (60):pii:3774. doi: 10.3791/3774.

Sun T, Walsh CA. 2006. Molecular approaches to brain asymmetry and handedness. Nat Rev Neurosci. 7:655–662.

Takahashi K, Saleh M, Penn RD, Hatsopoulos NG. 2011. Propagating waves in human motor cortex. Front Hum Neurosci. 5:40.

Tanner D, Morgan-Short K, Luck SJ. 2015. How inappropriate high-pass filters can produce artifactual effects and incorrect conclusions in ERP studies of language and cognition. Psychophysiology. 52:997–1009.

Tiriac A, Uitermarkt BD, Fanning AS, Sokoloff G, Blumberg MS. 2012. Rapid whisker movements in sleeping newborn rats. Curr Biol. 22:2075–2080.

Tolner EA, Sheikh A, Yukin AY, Kaila K, Kanold PO. 2012. Subplate neurons promote spindle bursts and thalamocortical patterning in the neonatal rat somatosensory cortex. J Neurosci. 32(2):692–702.

Tritsch NX, Yi E, Gale JE, Glowatzki E, Bergles DE. 2007. The origin of spontaneous activity in the developing auditory system. Nature. 450(7166):50–55.

Tritsch NX, Rodríguez-Contreras A, Crins TT, Wang HC, Borst JG, Bergles DE. 2010. Calcium action potentials in hair cells pattern auditory neuron activity before hearing onset. Nat Neurosci. 13(9):1050–1052.

Tuncdemir SN, Wamsley B, Stam FJ, Osakada F, Goulding M, Callaway EM, Rudy B, Fishell G. 2016. Early somatostatin interneuron connectivity mediates the maturation of deep layer cortical circuits. Neuron. 89:521–535.

Vanhatalo S, Palva JM, Andersson S, Rivera C, Voipio J, Kaila K. 2005. Slow endogenous activity transients and developmental expression of K+-Cl- cotransporter 2 in the immature human cortex. Eur J Neurisci. 22:2799–2804.

Vanhatalo S, Kaila K. 2006. Development of neonatal EEG activity: from phenomenology to physiology. Semin Fetal Neonatal Med. 11(6):471–478.

Weitzman L, Graziani L, Duhamel L. 1967. Maturation and topography of the auditory-evokedresponse of the prematurely born infant. Electroencephalogr Clin Neurophysiol. 23:82–83.

Widmann A, Schröger E, Maess B. 2015. Digital filter design for electrophysiological data–a practical approach. J Neurosci Methods. 250:34–46.

Wolters CH, Anwander A, Tricoche X, Weinstein D, Koch MA, MacLeod RS. 2006. Influence of tissue conductivity anisotropy on EEG/MEG field and return current computation in a realistic head model: a simulation and visualization study using high-resolution finite element modeling. Neuroimage. 30:813–826.

Workman AD, Charvet CJ, Clancy B, Darlington RB, Finlay BL. 2013. Modeling transformations of neurodevelopmental sequences across mammalian species. J Neurosci. 33: 7368–7383.

Woods DL, Herron TJ, Cate AD, Kang X, Yund EW. 2011. Phonological processing in human auditory cortical fields. Front Hum Neurosci. 5:42.

Wunderlich JL, Cone-Wesson BK. 2006. Maturation of CAEP in infants and children: a review. Hear Res. 212:212–223.

Yang JW, Hanganu-Opatz IL, Sun JJ, Luhmann HJ. 2009. Three patterns of oscillatory activity differentially synchronize developing neocortical networks in vivo. J Neurosci. 29:9011–9025.

Yang JW, An S, Sun JJ, Reyes-Puerta V, Kindler J, Berger T, Kilb W, Luhmann HJ. 2013. Thalamic network oscillations synchronize ontogenetic columns in the newborn rat barrel cortex. Cereb Cortex. 23:1299–1316.

Yang JW, Reyes-Puerta V, Kilb W, Luhmann HJ. 2016. Spindle bursts in neonatal rat cerebral cortex. Neural Plast. 2016: 3467832.

Wang HC, Lin CC, Cheung R, Zhang-Hooks Y, Agarwal A, Ellis-Davies G, Rock J, Bergles DE. 2015. Spontaneous activity of cochlear hair cells triggered by fluid secretion mechanism in adjacent support cells. Cell. 163(6):1348–1359.

Zatorre RJ, Bouffard M, Ahad P, Belin P. 2002. Where is 'where' in the human auditory cortex? Nat Neurosci. 5:905–909.